Hydrogen-Bonded Porphyrinic Solids: Supramolecular Networks of Octahydroxy Porphyrins

P. Bhyrappa, Scott R. Wilson, and Kenneth S. Suslick*

Contribution from the Department of Chemistry, University of Illinois at Urbana−Champaign, 601 South Goodwin Avenue, Urbana, Illinois 61801

Received April 7, 1997[⊗]

Abstract: Symmetrically substituted octahydroxy porphyrins, tetrakis(3′,5′-dihydroxyphenyl)porphyrin, H_2T(3′,5′-DHP)P, tetrakis(2′,6′-dihydroxyphenyl)porphyrin, H_2T(2′,6′-DHP)P, and their Zn(II) and Mn(III) derivatives have been developed as building blocks for supramolecular hydrogen-bonded networks. The crystal structures of a series of these porphyrins exhibit unique structural features through assembly of porphyrin networks by means of directional hydrogen bonding. The position of the peripheral hydroxyl groups, the choice of metallo- or free base porphyrin, and the nature of the solvate (i.e., guest) dramatically influence structural features. A one-dimensional, columnar structure is found for H_2T(3′,5′-DHP)P·5EtOAc. With benzonitrile as solvate, the structure of H_2T(3′,5′-DHP)P·7C_6H_5-CN changes substantially to a three-dimensional corrugated-sheet structure in order to accommodate a larger pore size. When the hydroxyl substituents are simply changed from the *m*- to the *o*-phenyl positions, an essentially two-dimensional layered structure is formed for H_2T(2′,6′-DHP)P·4EtOAc. Zn[T(2′,6′-DHP)P](EtOAc)$_2$·2EtOAc has a two-dimensional layered structure, similar to that of its free base H_2T(2′,6′-DHP)P interaction between the aryl rings of the adjacent layers. The crystal structures of both Zn[T(3′,5′-DHP)P] and Mn[T(3′,5′-DHP)P](Cl) exhibited three-dimensional hydrogen-bonding features. Zn[T(3′,5′-DHP)P](THF)$_2$·2THF·3CH_2Cl_2 has a three-dimensional interconnected layered structure with metalloporphyrins arranged in a slipped stack orientation within the layers. In the structure of Mn[T(3′,5′-DHP)P](THF)$_2$.Cl·2THF·5$C_6H_5CH_3$, a chloride anion dictates the three-dimensional packing by bridging four metalloporphyrin molecules through Cl···HO bonding interactions. In all of these structures, large solvate-filled channels are present with cross-sections as large as 42 Å^2. The pore volumes of these channels are exceptionally large: as much as 67% of the unit cell volume.

Introduction

In recent years there has been an increasing interest in nanoporous molecular crystalline solids and their various applications.[1] Of special importance is the development of molecular building blocks for the design and crystal engineering of such materials. A wide variety of organic molecules have been engineered for generating nanoporous crystalline materials.[1] Porphyrins and metalloporphyrins provide a relatively unexplored class of such building blocks because of their large size, ease of synthesis, excellent thermal stability, and diversity of their coordination and catalytic chemistry. Furthermore, porphyrins provide an extremely versatile platform on which to build desired peripheral functionality with designed orientations. Such functionality can provide the intermolecular interactions that control self-assembly both in solution and in the solid state. There have been a few recent reports on the supramolecular architectures of porphyrin solids with hydrogen-bonded[2] and metal−organic coordination[3] networks. In addition, the extensive structural work that exists for porphyrins and metalloporphyrins[4] provides a database for the systematic examination of intermolecular interactions in the solid state. Notably, Strouse and co-workers[5] have reported a wide range of clathrate-like host/guest solid state structures of H_2TPP and its metal derivatives. *meso*-Tetraphenylporphyrins are the most widely used systems due to their ease of synthesis and facile functionalization.

In order to more rationally control the structure of porphyrinic solids, we prepared a family of symmetric octahydroxy-substituted porphyrins and their metal complexes, wherein the three-dimensional structure is determined by the directional hydrogen bonding of hydroxyl groups. We report here the synthesis of two octahydroxy porphyrins,[6] H_2T(3′,5′-DHP)P and H_2T(2′,6′-DHP)P, and their Zn(II) and Mn(III) derivatives (Figure 1) as building blocks for the synthesis of hydrogen-bonded crystalline solids, together with six X-ray structures derived from these porphyrins; this paper is an extension of our preliminary communication of the free base porphyrin structures.[6b] Several structural architectures in the packing of these porphyrins have been observed and are discussed below in some detail. The use of hydroxy substitution, combined with the rigidity and high symmetry of the porphyrinic building blocks, leads to the formation of highly open structures with large void volumes.

[⊗] Abstract published in *Advance ACS Abstracts,* August 15, 1997.

(1) Bein, T., Ed.; *Supramolecular Architecture*; ACS Symposium Series; American Chemical Society: Washington, DC, 1992; Vol. 499, pp 88−253. (b) Komarneni, S.; Smith, D. M.; Beck, J. S. Ed.; *Advances in Porous Materials*; Materials Research Society: Pittsburgh, PA, 1995. (c) Yaghi, O. M.; Li, G.; Li, H. *Nature* **1995**, *378*, 703. (d) Yaghi, O. M.; Hailian, L.; Groy, T. L. *J. Am. Chem. Soc.* **1996**, *118*, 9096 and references cited therein. (e) Venkataraman, D.; Garner, G. B.; Lee, S.; Moore, J. S. *J. Am. Chem. Soc.* **1996**, *118*, 9096.

(2) Goldberg, I.; Kruptitsky, H.; Stein, Z.; Hsiou, Y.; Strouse, C. E. *Supramol. Chem.* **1995**, *4*, 203 and references cited therein.

(3) (a) Abrahams, B. F.; Hoskins, B. F.; Michall, D. M.; Robson, R. *Nature* **1994**, *369*, 727. (b) Abrahams, B. F.; Hoskins, B. F.; Michall, D. M.; Robson, R. *J. Am. Chem. Soc.* **1991**, *113*, 3606.

(4) Scheidt, W. R.; Lee, Y. J. *Struct. Bond. (Berlin)* **1987**, *64*, 1.

(5) Byrn, M. P.; Curtis, C. J.; Hsiou, Y.; Khan, S. I.; Sawin, P. I.; Tendick, S. K.; Terzis, A.; Strouse, C. E. *J. Am. Chem. Soc.* **1993**, *115*, 9480 and references cited therein. (b) Krupitsky, H.; Stein, S.; Goldberg, I. *J. Inclusion Phenom. Mol. Recognit. Chem.* **1995**, *20*, 211. (c) Krupitsky, H.; Stein, S.; Goldberg, I. Strouse, C. E. *J. Inclusion Phenom. Mol. Recognit. Chem.* **1994**, *18*, 177.

(6) (a) Abbreviations: T(2′,6′-DMP)P, 5,10,15,20-tetrakis(2′,6′-dimethoxyphenyl)porphyrinate(−2); T(2′,6′-DHP)P, 5,10,15,20-tetrakis(2′,6′-dihydroxyphenyl)porphyrinate(−2); T(3′,5′-DMP)P, 5,10,15,20-tetrakis(3′,5′-dimethoxyphenyl)porphyrinate(−2); T(3′,5′-DHP)P, 5,10,15,20-tetrakis-(3′,5′-dihydroxyphenyl)porphyrinate(−2); EtOAc, ethyl acetate; THF, tetrahydrofuran. (b) Bhyrappa, P; Wilson, S. R.; Suslick, K. S. *Supramol. Chem.* In press.

S0002-7863(97)01093-7 CCC: $14.00

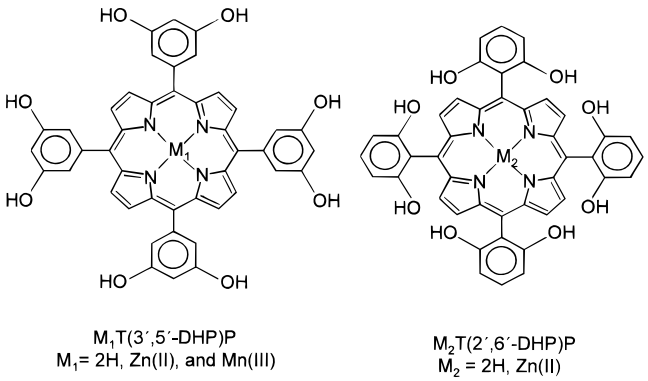

Figure 1. Chemical structures of octahydroxy porphyrins, $H_2T(3',5'$-DHP)P and $H_2T(2',6'$-DHP)P, and their metal derivatives.

Experimental Section

Materials. Octamethoxy porphyrins, 5,10,15,20-tetrakis(2′,6′-dimethoxyphenyl)porphyrin,[7a] $H_2T(2',6'$-DMP)P, and 5,10,15,20-tetrakis(3′,5′-dimethoxyphenyl)porphyrin,[7b] $H_2T(3',5'$-DMP)P, were synthesized using reported procedures. 5,10,15,20-Tetrakis(3′,5′-dihydroxyphenyl)porphyrin, $H_2T(3',5'$-DHP)P, was prepared using literature method.[7] Demethylation of $H_2T(2',6'$-DMP)P was unsuccessful with BBr_3 and was carried out using pyridinium hydrochloride at 220 °C under N_2.[8] Zinc complexes, Zn[T(2′,6′-DHP)P] and Zn[T(3′,5′-DHP)P], were prepared by metallation in the usual fashion.[9] Dichloromethane, purchased from Fisher was distilled over CaH_2 under nitrogen before use. Ethyl acetate was purchased from Fisher and used as received. Toluene obtained from Fisher was distilled over sodium under nitrogen before use. Tetrahydrofuran was predried from 4 Å molecular sieves and distilled from sodium/benzophenone under nitrogen before use. *n*-Heptane and benzonitrile, C_6H_5CN, obtained from Aldrich were used as received.

Synthesis of 5,10,15,20-tetrakis(2′,6′-dihydroxyphenyl)porphyrin, $H_2T(2',6'$-DHP)P. Demethylation of $H_2T(2',6'$-DMP)P was carried out using reported procedures[8] with slight modifications. To a Schlenk flask containing $H_2T(2',6'$-DMP)P (0.38 g, 0.5 mmol) was added pyridinium hydrochloride (20.0 g, 0.17 mol). The reaction mixture was stirred and refluxed (200−220 °C) under Ar for 2 h. At the end of this period, the mixture was cooled to room temperature and poured into water (500 mL). The porphyrin was extracted with ethyl acetate. The organic layer was washed twice with hydrochloric acid (0.1 M) followed by saturated aqueous $NaHCO_3$ solution and dried over anhydrous Na_2SO_4. The resulting solution was concentrated and chromatographed on a silica gel column using 20% THF in ethyl acetate as the eluent. The yield of the product was 0.25 g (75%). Anal. Calcd for $C_{44}H_{30}N_4O_8 \cdot H_2O$: C, 69.47; H, 4.24; N, 7.36. Found: C, 69.70; H, 4.25; N, 7.18. ^{1}H NMR in CD_3CN: −2.75 (s, 2H, imino-H), 7.2−7.8 (12H, m, phenyl-H), and 8.85 (8H, s, pyrrole-H) ppm.

Synthesis of 5,10,15,20-Tetrakis(3′,5′-dihydroxyphenyl)porphinatomanganese(III) Chloride, Mn[T(3′,5′-DHP)P](Cl). This complex was prepared using variant of reported procedure.[10] To a DMF (30 mL) solution containing (0.2 g, 0.25 mmol) $H_2T(3',5'$-DHP)P was added anhydrous $MnCl_2$ (0.5 g, 3.9 mmol), and the solution was refluxed for a period of 6 h. At the end of this period, DMF was removed under reduced pressure. The residue thus obtained was redissolved in ethyl acetate and washed with distilled water to remove excess $MnCl_2$. The product was recrystallized from 1:1 mixture of THF/CH_2Cl_2 and dried under vacuum at 100 °C for 12 h. The yield of the product was found to be 0.12 g (65%). Anal. Calcd. for $C_{44}H_{28}N_4O_8MnCl$: C, 63.61; H, 3.40; N, 6.75; Mn, 6.62; Cl, 4.21%. Found: C, 63.10; H, 3.30; N, 6.65; Mn, 6.40; Cl, 4.30. UV−vis absorption spectrum in THF, λ_{max}: 375, 395, 479, 523, 584, and 623 nm. Negative ion electrospray mass spectrum: calcd (*m/e*) for $[M - Cl]^+$, 795.67; found, 794.90.

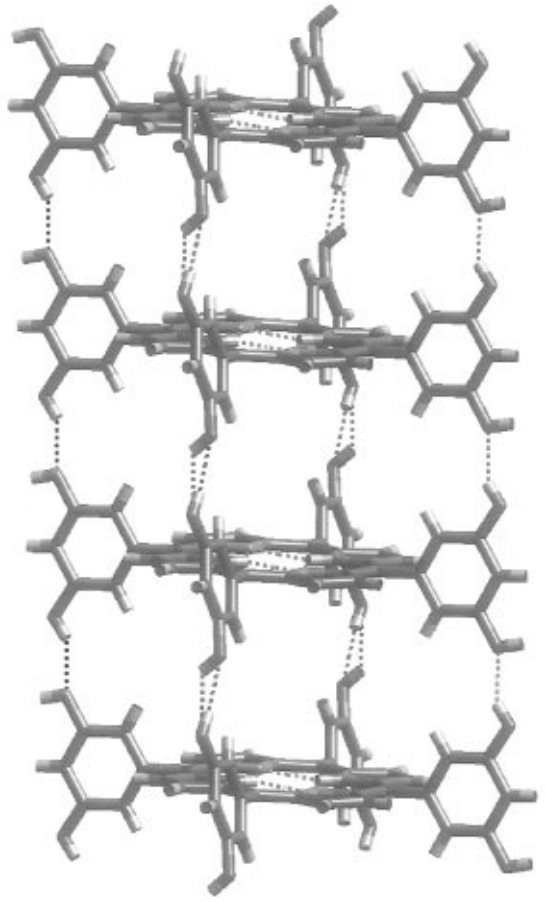

Figure 2. Molecular packing diagram of $H_2T(3',5'$-DHP)P·6EtOAc showing one-dimensional columnar structure. Hydrogen-bonding interactions between the hydroxyl groups are shown with dotted lines.

Crystallization. Porphyrin crystals were grown by liquid diffusion of a second solvent into a porphyrin solution. For $H_2T(3',5'$-DHP)P·5EtOAc, $H_2T(3',5'$-DHP)P·$7C_6H_5CN$, $H_2T(2',6'$-DHP)P·4EtOAc, and Zn[T(2′,6′-DHP)P](EtOAc)$_2$·2EtOAc, crystals were grown by direct diffusion of *n*-heptane into a EtOAc (or benzonitrile) porphyrin solution. For Mn[T(3′,5′-DHP)](THF)$_2$·Cl·2THF·$5C_6H_5CH_3$, toluene was allowed to diffuse slowly over a period of roughly 3 days into a saturated solution of Mn[T(3′,5′-DHP)P](Cl) in THF. Crystals of Zn[(T(3′,5′-DHP)P](THF)$_2$·2THF·$3CH_2Cl_2$ were grown by direct diffusion of CH_2Cl_2 into a saturated solution of Zn[T(3′,5′-DHP)P] in THF. All crystallization procedures were carried out at room temperature. The crystals employed in this study were found to lose solvates upon removal from the mother liquor, and subsequent loss of crystallinity occurred. Attempts to replace solvate into dried solids by vapor diffusion resulted in partial resolvation (based on thermogravimetric data) in some but not all cases.

X-ray Data Collection. The X-ray diffraction data were collected on a automated Enraf-Nonius CAD-4 diffractometer. Single crystals were covered with oil (Paratone-N, Exxon), mounted on to a thin glass fiber, and then cooled to 198 K to prevent solvate loss. Porphyrin crystals tend to lose crystallinity upon removal from mother liquor at room temperature. Intensity data was collected by $\omega-2\theta$ mode in the range of 1.0−23° at 198 K. Three standard intensities were monitored for every 90 min and showed 1.6, 0.8, 0.54, and 0.5% decay for $H_2T(3',5'$-DHP)P·5EtOAc, $H_2T(3',5'$-DHP)P·$7C_6H_5CN$, Zn[T(3′,5′-DHP)P](THF)$_2$·2THF·$3CH_2Cl_2$, and Mn[T(3′,5′-DHP)P](THF)$_2$·Cl·2THF·$5C_6H_5CH_3$ crystals, respectively. No intensity decay was observed for $H_2(2',6'$-DHP)P·4EtOAc and Zn[T(2′,6′-DHP)P](EtOAc)$_2$·2EtOAc crystals. No decay corrections were applied.

Crystal structure data for $H_2T(3',5'$-DHP)P·5EtOAc: red prismatic crystals; $C_{64}H_{70}N_4O_{18}$, $M = 1183.24$, triclinic, $P\bar{1}$, $a = 7.245(2)$ Å, $b = 14.727(3)$ Å, $c = 14.835(4)$ Å, $\alpha = 90.18(2)°$, $\beta = 92.90(2)°$, $\gamma = 90.02(2)°$, $V = 1580.8(7)$ Å^3, $Z = 1$. The structure was refined

(7) (a) Tsuchida, E.; Komatsu, T.; Hasegava, E.; Nishide, H. *J. Chem. Soc., Dalton Trans*. **1990**, 2713. (b) Jin, R.-H.; Aida, T.; Inoue, S. *J. Chem. Soc., Chem. Commun*. **1993**, 1260.

(8) Momenteau, M.; Mispelter, J.; Loock, B.; Bisagni, E. *J. Chem. Soc., Perkin Trans. 1* **1983**, 189.

(9) Dorough, G. D.; Miller, J. R.; Huennekens, F. M. *J. Am. Chem. Soc*. **1948**, *70*, 1808.

(10) Jones, R. D.; Summerville, D. A.; Basolo, F. *J. Am. Chem. Soc.* **1978**, *100*, 4416.

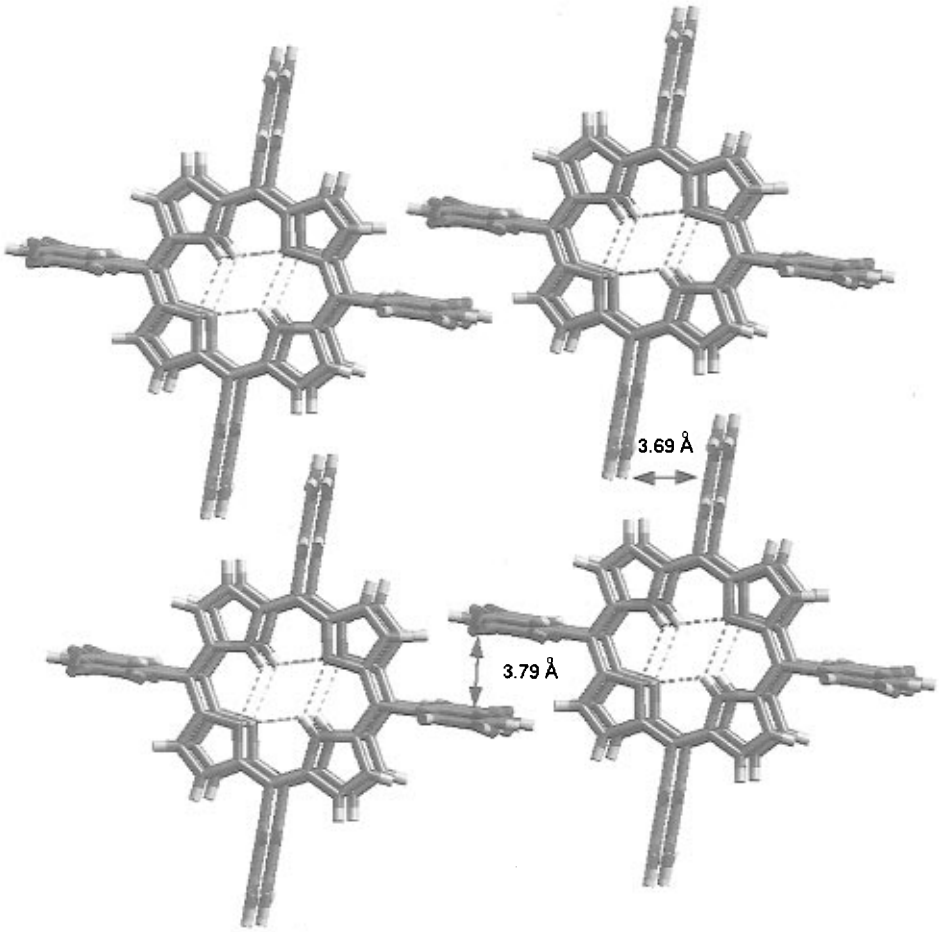

Figure 3. Crystal packing modes showing close contact and a channel for $H_2T(3',5'\text{-DHP})P\cdot 5EtOAc$. Solvent molecules are not shown for clarity.

using full-matrix least-squares on F_o^2 (data/restraints/parameters 4369:336:391), converging to $R_1 = 0.1138$, wR2 = 0.2801 (on 2588, $I > 2\sigma(I)$ observed data). The solvate molecules were highly disordered.

Crystal structure data for $H_2T(3',5'\text{-DHP})P\cdot 7C_7H_5N$: purple plate-like crystals; $C_{93}H_{65}N_{11}O_8$, $M = 1464.56$, monoclinic, $P2_1/m$, $a = 11.105(4)$ Å, $b = 25.744(7)$ Å, $c = 14.022(3)$ Å, $\beta = 108.09(2)°$, V = 3811(2) Å^3, $Z = 2$. The structure was refined using full-matrix least-squares on F_o^2 (data/restraints/parameters 6106:0:548), converging to $R_1 = 0.0622$, wR2 = 0.1305 (on 2588, $I > 2\sigma(I)$ observed data).

Crystal structure data for $H_2T(2',6'\text{-DHP})P\cdot 4EtOAc$: purple prismatic crystals; $C_{60}H_{62}N_4O_{16}$, $M = 1095.14$, triclinic, $P\bar{1}$, $a = 13.736(3)$ Å, $b = 14.032(3)$ Å, $c = 17.029(3)$ Å, $\alpha = 93.77(3)°$, $\beta = 110.92(3)°$, $\gamma = 111.81(3)°$, $V = 2770.9(10)$ Å^3, $Z = 2$. The structure was refined using full-matrix least-squares on F_o^2 (data/restraints/parameters 8624:64:846), converging to $R_1 = 0.0457$, wR2 = 0.1129 (on 6260, $I > 2\sigma(I)$ observed data).

Crystal structure data for $Zn[T(2',6'\text{-DHP})P](EtOAc)_2\cdot 2EtOAc$: red prismatic crystals; $C_{60}H_{60}N_4O_{16}Zn$, $M = 1158.49$, triclinic, $P\bar{1}$, $a = 10.599(3)$ Å, $b = 11.301(4)$ Å, $c = 12.535(6)$ Å, $\alpha = 85.70(4)°$, $\beta = 70.19(4)°$, $\gamma = 79.15(3)°$, $V = 1387.2(9)$ Å^3, $Z = 1$. The structure was refined using full-matrix least-squares on F_o^2 (data/restraints/parameters 3850:20:371), converging to $R_1 = 0.0984$, wR2 = 0.2527 (on 2610, $I > 2\sigma(I)$ observed data).

Crystal structure data for $Zn[T(3',5'\text{-DHP})P](THF)_2\cdot 2THF\cdot 3CH_2Cl_2$: purple, plate-like crystals; $C_{63}H_{66}N_4Cl_6O_{12}Zn$, $M = 1349.27$, triclinic, $P\bar{1}$, $a = 10.212(3)$ Å, $b = 12.365(3)$ Å, $c = 14.628(3)$ Å, $\alpha = 99.71(2)°$, $\beta = 108.52(2)°$, $\gamma = 107.49(2)°$, $V = 1597.6(7)$ Å^3, $Z = 1$. The structure was refined using full-matrix least-squares on F_o^2 (data/restraints/parameters 5585:255:528), converging to $R_1 = 0.0679$, wR2 = 0.1889 (on 4121, $I > 2\sigma(I)$ observed data).

Crystal structure data for $Mn[T(3',5'\text{-DHP})P](THF)_2\cdot Cl\cdot 2THF\cdot 5C_6H_5CH_3$: purple, tabular crystals; $C_{95}H_{100}N_4Cl\,MnO_{12}$, $M = 1580.18$, monoclinic, $P2_1/n$, $a = 13.937(4)$ Å, $b = 16.443(5)$ Å, $c = 19.541(6)$ Å, $\alpha = 90°$, $\beta = 106.71(2)°$, $\gamma = 90°$, $V = 4289(2)$ Å^3, $Z = 2$. The structure was refined using full-matrix least-squares on F_o^2 (data/restraints/parameters 5942:226:567), converging to $R_1 = 0.0797$, wR2 = 0.1742 (on 2568, $I > 2\sigma(I)$ observed data).

Structure Analysis and Refinement. Structures were solved by direct methods (SHELXS).[11a] In all cases, porphyrin macrocycle non-H-atoms were deduced from an E-map. For all structures, one cycle of isotropic least-squares refinement followed by an unweighted difference Fourier synthesis revealed positions for ordered atoms. H atoms and disordered solvate molecules were idealized. Successful convergence of the full-matrix least-squares refinement on F^2 (SHELXL)[11b] was indicated by the maximum shift/error for the cycle. Final difference electron density maps for $Zn[T(3',5'\text{-DHP})P](THF)_2\cdot 2THF\cdot 3CH_2Cl_2$ and $Zn[T(2',6'\text{-DHP})P](EtOAc)_2]\cdot 2EtOAc$ structures showed a residual density of 1.05 and 1.43 e Å^{-3} in the vicinity of disordered solvate molecules, respectively. Final difference electron-density maps were featureless. Molecular modeling of porphyrins and solvent molecules were performed on a Silicon Graphics Indigo^2 Extreme workstation using Cerius,^{2} Quanta 4.0, and CHARMm software package.

Results and Discussion

In order to more rationally control the structure of porphyrinic solids, we have examined a pair of symmetric polysubstituted porphyrins, wherein the three-dimensional structure is determined by the directional hydrogen bonding of eight hydroxyl groups per porphyrin. To this end, we have examined two *meso*-tetraaryl porphyrins, with four dihydroxyphenyl groups either *m*- or *o*-substituted: $H_2T(3',5'\text{-DHP})P$ and $H_2T(2',6'\text{-DHP})P$, and their Zn(II) and Mn(III) derivatives with several different solvates (Figure 1). The characteristic solid state structural features of these octahydroxy porphyrins are dictated by

(11) (a) Sheldrick, G. M. SHELXS-86. *Acta Crystallogr.* **1990**, *A46*, 467. (b) Sheldrick, G. M. SHELXL-93. *Program for the Refinement of Crystal Structures from Diffraction Data;* University of Goettingen, Germany, 1993.

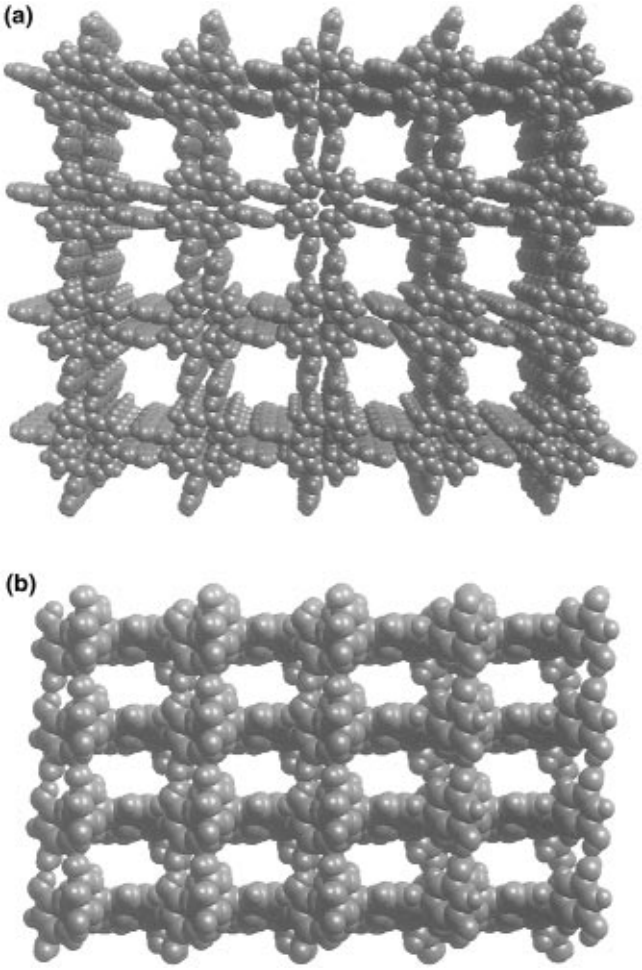

Figure 4. Molecular packing diagrams of H_2T(3′,5′-DHP)P·5EtOAc (van der Waals spheres shown at 0.7 of atomic radii): (a) showing channels of 6.5 Å by 6.5 Å, between the columns; (b) showing channels of 3.4 Å × 3.4 Å running perpendicular to the columns. Solvent molecules are not shown for clarity. Distances shown for the channels exclude van der Waals radii of 3.6 Å.

directional hydrogen bonding. This can lead to one-dimensional columnar structures, two-dimensional sheet structures, and three-dimensional networks. The order of discussion below follows the increasing dimensionality of these solid state structures. As a consequence of the constraints that the hydrogen-bonding networks impose, the solids of these complexes have very large amounts of solvate molecules in the lattice relative to previously known porphyrin crystals:[2,5] in some cases, as many as seven solvates per porphyrin, with lattice solvate volume occupying as much as two-thirds of the total.

(A) Free Base Porphyrin Structures. To delineate the effect of substituent position on the crystal packing and porosity of the structure, diffraction quality crystals of H_2T(3′,5′-DHP)P and H_2T(2′,6′-DHP)P were obtained with the same lattice guest, ethyl acetate. The observed bond lengths and bond angles for the porphyrin macrocycle are not significantly different from that of the *meso*-tetraphenylporphyrin.[20]

H_2T(3′,5′-DHP)P·5EtOAc. As shown in Figure 2, H_2T(3′,5′-DHP)P·5EtOAc shows an essentially one-dimensional columnar structure and the unit cell has one porphyrin with five EtOAc molecules. The structure is controlled by the presence of strong, directional hydrogen bonding between the *meso*-(phenylhydroxyl) groups. The phenyl rings are roughly perpendicular to the porphyrin plane with angles of 70−85°. To optimize hydrogen-bonding interactions, the porphyrin macrocycles are almost planar and are nearly eclipsed with respect to one another within each of the columns. Hydrogen bonding exists only

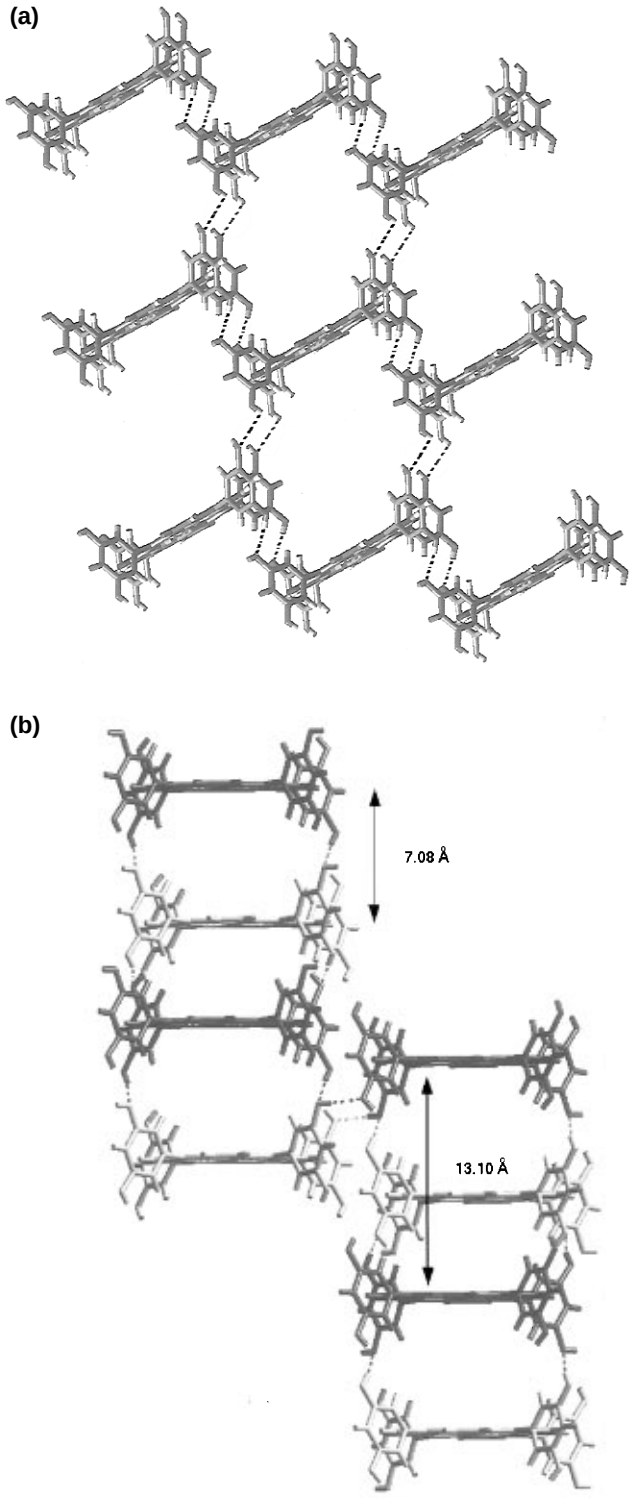

Figure 5. Depicts the molecular packing of H_2T(3′,5′-DHP)P·7C_6H_5-CN complex. Hydrogen bonds are shown in dotted lines. (a) Corrugated two-dimensional layer of hydrogen-bonded porphyrins. (b) Interconnections by hydrogen bonding between layers. The porphyrins in dark and light shades indicate front and back, respectively.

between each porphyrin and its nearest neighbor above and below within the column, with an interporphyrin plane separation of 7.0 Å and negligible $\pi-\pi$ interactions between the macrocycles. The average O···O separation between hydrogen-bonded OH groups was found to be 2.68 Å, indicative of strong directional hydrogen bonding and comparable to previously reported structures.[2]

As shown in Figure 3, the columns stack parallel to one another, forming a porous network in H_2T(3′,5′-DHP)P·5EtOAc. There is no hydrogen bonding between columns, instead the

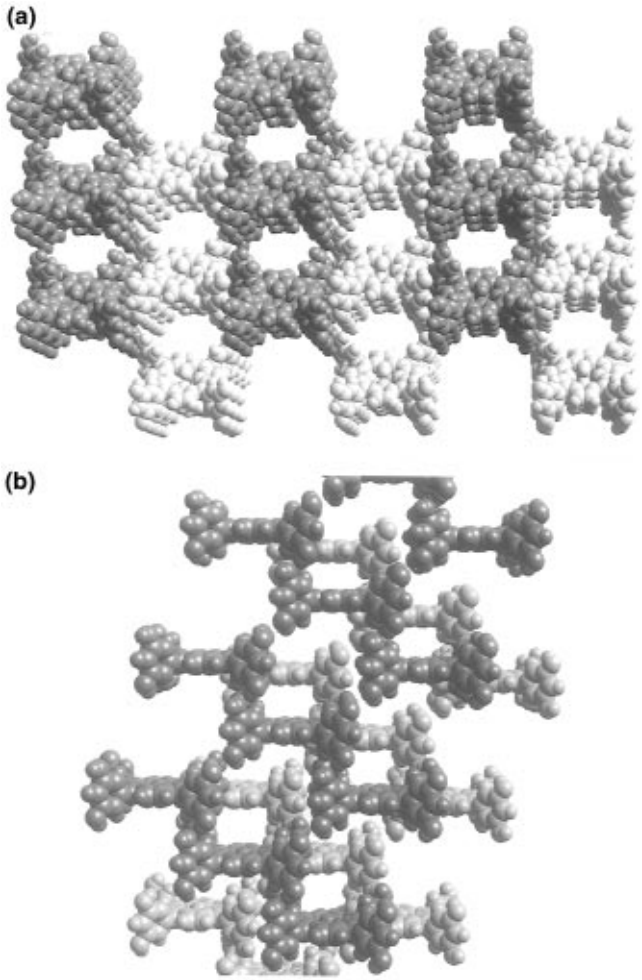

Figure 6. Molecular packing diagrams of $H_2T(3',5'\text{-DHP})P\cdot 7C_6H_5CN$: (a) showing channels of 5.5 Å × 6.0 Å (molecules shown in light and dark shades indicates different one-dimensional corrugated sheets); (b) showing 4.0 Å × 5.0 Å wide channels running approximately perpendicular to the channels shown in Figure 6a (molecules shown in dark and light shades indicate front and farther away, respectively). Atoms are drawn at 70% of their VDW atomic radii. Solvate molecules are not shown for clarity.

columns are held together by weak van der Waals forces. The closest intercolumnar phenyl−phenyl ring separations are at 3.79 and 3.69 Å, which indicate only limited $\pi-\pi$ interaction between them. The center-to-center distance between the adjacent porphyrins of the neighboring columns is 14.83 Å. Four columns form a large solvate-filled channel of 6.5 Å × 6.5 Å (van der Waals surface to van der Waals surface), i.e., a cross-sectional area of 42 Å^2 (Figure 4a). There are two smaller channels (3.4 Å × 3.4 Å) running perpendicular to each other and perpendicular to the columns, as shown in Figure 4b. The solvent molecules show some disorder and are free of any hydrogen-bonding interactions.

$H_2T(3',5'\text{-DHP})P\cdot 7C_6H_5CN$. For examination of the effect of the solvate on the molecular packing in these systems, crystals of $H_2T(3',5'\text{-DHP})P$ were grown from benzonitrile, a much larger solvate molecule. The solid state structure of $H_2T(3',5'\text{-DHP})P\cdot 7C_6H_5CN$ is dramatically altered by the benzonitrile (Figure 5). The structure has changed from a one-dimensional columnar structure (for ethyl acetate) to a three-dimensional corrugated slipped-stack structure, with a pore size matched to the benzonitrile. Two corrugated sheets (Figure 5a) are interconnected by a third, which forms the observed three-dimensional structure. The unit cell contains 2 planar porphyrin molecules and 14 benzonitrile solvate molecules. Molecular packing diagrams (Figure 6) show two solvate-filled channels perpendicular to each other with sizes of 5.5 Å × 6.0 Å (i.e., cross-sectional area 33 Å^2) and 4.0 Å × 5.0 Å, respectively. Porphyrin molecules are arranged in an offset fashion to favor hydrogen-bonding interactions at the expense of $\pi-\pi$ interactions.

In the structure of $H_2T(3',5'\text{-DHP})P\cdot 7C_6H_5CN$, each porphyrin is hydrogen bonded to three closest neighbor porphyrins. The center-to-center distance between the adjacent layers is about 12.6 Å, and the vertical distance between nearest hydrogen-bonded porphyrins is 7.4 Å. Porphyrins are arranged in an offset fashion within the sheet to maximize hydrogen bonding between the OH groups, with a mean porphyrin−porphyrin vertical separation of 7.08 Å. Within the layer, the average O···O distance between the hydrogen-bonded OH groups is 2.85 Å. The largest vertical separation between the two nearest neighbors in a given sheet is 13.10 Å. The two corrugated layers are held together by means of hydrogen bonding (OH···OH) with a mean O···O distance of 2.73 Å. Hydrogen bonding between the porphyrins is partially disrupted by the benzonitrile due to hydrogen bonding from the porphyrin hydroxyl groups to nitriles of the solvates with an average O···N distance of 2.85 Å. Two benzonitrile molecules are located above the porphyrin plane with a mean plane separation of 3.60 Å. The closest separation between the neighboring porphyrin phenyl rings is 3.44 Å.

$H_2T(2',6'\text{-DHP})P\cdot 4EtOAc$. When the position of the hydroxyl substituents is changed from the *m*- to the *o*- positions of the phenyl rings, a substantial change in the structure occurs: $H_2T(2',6'\text{-DHP})P\cdot 4EtOAc$ has a two-dimensional layered structure, as shown in the molecular packing diagram in Figure 7. The unit cell has two porphyrins, each with four ethyl acetate molecules. The porphyrin rings are slightly ruffled and show strong directional hydrogen bonding induced by the peripheral hydroxyl groups. Each porphyrin has four hydrogen-bonded nearest neighbors in an offset orientation. The average hydrogen-bonding distance (O···O) is 2.79 Å. In a given layer, the vertical distance between the offset porphyrins is 7.0 Å. The center-to-center distance between the adjacent layers is 11.8 Å, and no hydrogen bonding occurs between the porphyrinic layers. This suggests a minimal interaction between the layers which are held together by van der Waals forces.

There exists an interesting interaction between the layers in $H_2T(2',6'\text{-DHP})P\cdot 4EtOAc$. *meso*-Aryl rings of the adjacent layers are at a mismatched orientation with one aryl C−H pointing into the middle of another aryl ring on a porphyrin in the adjacent layer. The slightly short distance of 3.33 Å from the aryl C−H to the adjacent porphyrin aryl-carbon indicates there is weak C−H···π interactions between the layers.[12] A channel of about 3.0 Å × 3.6 Å (van der Waals surface to van der Waals surface) runs along the layers and is filled with ethyl acetate molecules (Figure 8). Ethyl acetate molecules in the lattice are hydrogen bonded through their carbonyl groups to the hydroxyl groups of the porphyrins with an O···O average distance of 2.65 Å.

(B) Metalloporphyrin Structures. For examination of the effects of metallation on the structures and porosity of these octahydroxy porphyrins, Zn(II) and Mn(III) complexes were prepared and crystallized. These both form axially ligated complexes under crystallization conditions, which increases the steric demands of the porphyrin building block. For Zn(II)

(12) (a) Steiner, T. *J. Chem. Soc., Chem. Commun*. **1995**, 95. (b) Hunter, R.; Haueisen, R. H.; Irving, A. *Angew. Chem., Int. Ed. Engl*. **1994**, *33*, 566. (c) Desiraju, G. R. *Acc. Chem. Res*. **1996**, *29*, 441.

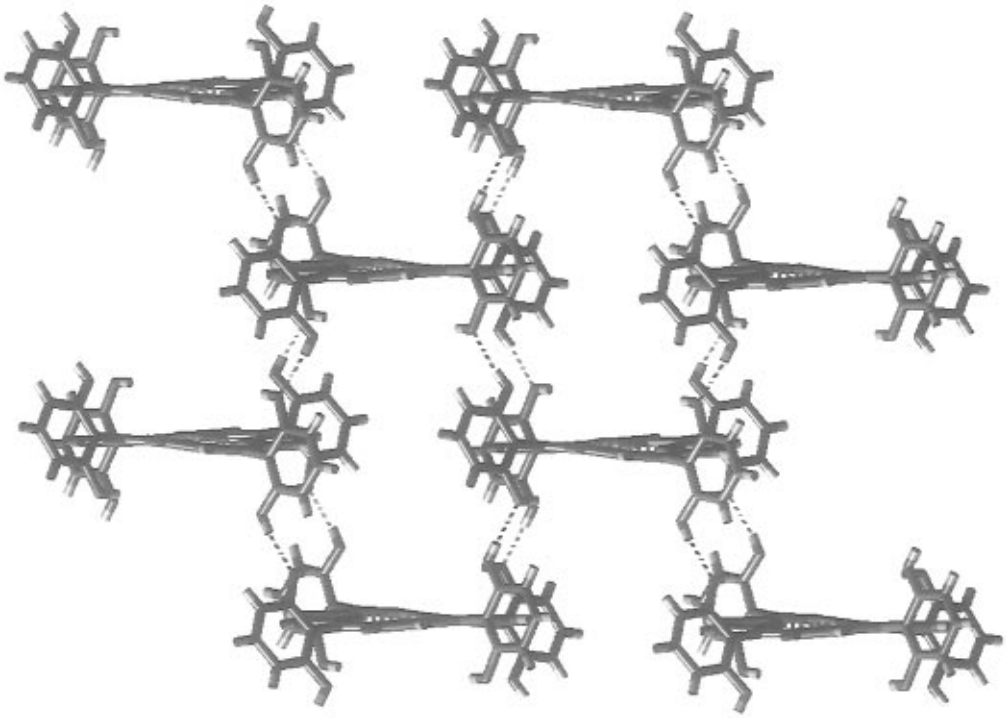

Figure 7. Molecular packing diagram of $H_2T(2',6'\text{-DHP})P\cdot 4EtOAc$ showing a two-dimensional layered structure. Hydrogen-bonding interactions between the hydroxyl groups are shown with dotted lines. Solvent molecules are not shown for clarity.

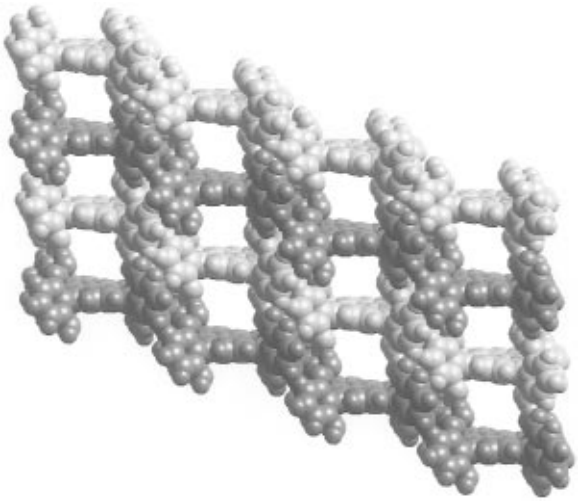

Figure 8. Molecular packing diagram of $H_2T(2',6'\text{-DHP})P\cdot 4EtOAc$ showing 3.0 Å × 3.6 Å wide channels along the layers. Space filling is shown at 0.7 of VDW atomic radii, and solvent molecules are not shown for clarity. Distances shown for the channels exclude van der Waals radii of 3.6 Å. The porphyrins in dark and light shades indicate that they are closer and further away, respectively.

metalloporphyrins, six-coordinate[13] complexes are less common than five-coordinate[4,14] ones. Mn(III) on the other hand generally forms six-coordinate complexes in the presence of excess ligands; in addition, the Mn(III) have a counteranion to place in the lattice as well. The observed bond lengths and bond angles for the metalloporphyrin macrocycles are not significantly different from those of similar metal complexes of the *meso*-tetraphenylporphyrin.

$Zn[T(2',6'\text{-DHP})P](EtOAc)_2\cdot 2EtOAc$. Crystals of $H_2T(2',6'\text{-DHP})P$ and $Zn[T(2',6'\text{-DHP})P](EtOAc)_2$ were prepared with the same solvate (i.e., guest) to delineate the effect of axial ligation on the crystal packing and structural porosity. As shown

(13) (a) Schauer, G. C.; Anderson, O. P.; Eaton, S. S.; Eaton, G. R. *Inorg. Chem.* **1985**, *24*, 4082. (b) Bhyrappa, P.; Krishnan, V.; Nethaji, M. *J. Chem. Soc., Dalton Trans.* **1993**, 1901.

(14) Collins, D. M.; Hoard, J. L. *J. Am. Chem. Soc.* **1970**, *92*, 3761.

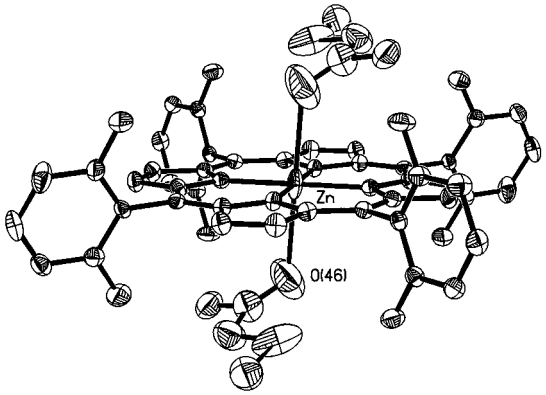

Figure 9. ORTEP diagram of the metalloporphyrin unit in the crystal structure of $Zn[T(2',6'\text{-DHP})P](EtOAc)_2\cdot 2EtOAc$

in Figure 9, the porphyrin ring is nearly planar in $Zn[T(2',6'\text{-DHP})P]$ while it is slightly ruffled in $H_2T(2',6'\text{-DHP})P$. It can be seen that both crystals have four ethyl acetates per porphyrin. The ethyl acetate molecules are hydrogen bonded to hydroxyl groups in $H_2T(2',6'\text{-DHP})P$, whereas for the Zn(II) complex, two ethyl acetate molecules are bonded to the metal center (Figure 9), while the other two are hydrogen bonded to the OH groups of the porphyrin. Axially ligated ethyl acetate molecules are in a *trans*-orientation and are bonded through the carbonyl oxygen of the ester with an average Zn−O distance of 2.532(3) Å. This rather long bond length may represent a crystallographic average of twin disordered five-coordinate complexes with the Zn atom out of the porphyrin plane closer to one ethyl acetate and with the second (*trans*) ethyl acetate only very loosely interacting. The large thermal parameters in the axial direction of the Zn and of the coordinated carbonyl oxygen make this a plausible explanation. Unfortunately, the Zn atom is at a center of inversion in this structure, so it is not possible to be more definitive. The average equatorial Zn−N distance is an unexceptional 2.043(2) Å.

The molecular packing structure of $Zn[T(2',6'\text{-DHP})P](EtOAc)_2\cdot 2EtOAc$ exhibits a two-dimensional layered structure (Figure 10) remarkably similar to that found in $H_2T(2',6'$-

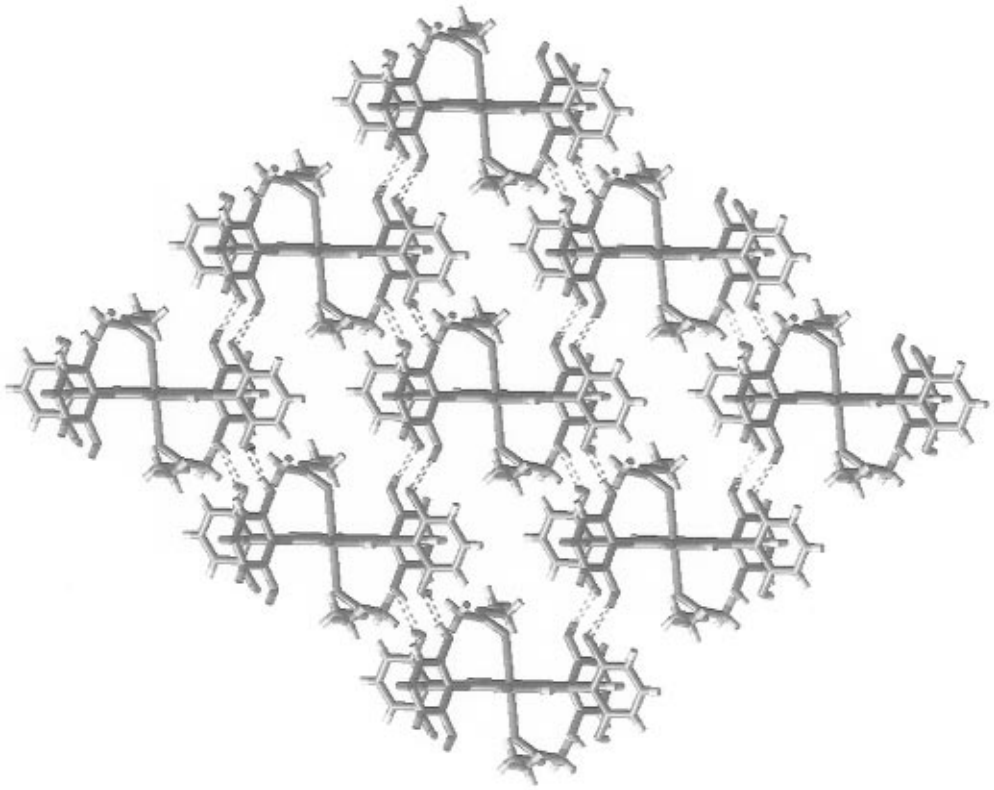

Figure 10. Molecular packing diagram of two-dimensional layered structure of Zn[T(2′,6′-DHP)P](EtOAc)$_2$·2EtOAc; a single plane of hydrogen-bonded porphyrin complexes is shown. The solvate (noncoordinated) molecules are not shown for clarity.

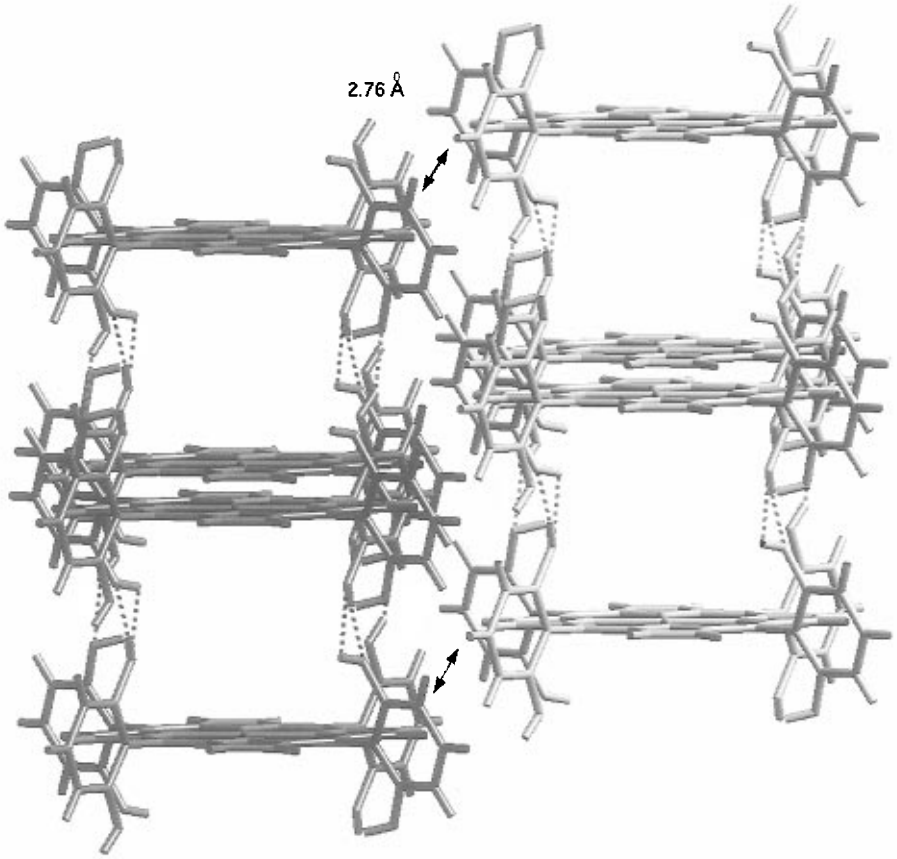

Figure 11. A perspective view of the Zn[T(2′,6′-DHP)P](EtOAc)$_2$·2EtOAc showing interlayer (C−H···π) interaction between layers. Coordinated ethyl acetate molecules are not shown for clarity. Hydrogen-bonding interactions are shown with dotted lines. Molecules shown in dark and light shades indicate front and farther away, respectively.

DHP)P·4EtOAc. The two noncoordinated EtOAc molecules are hydrogen bonded to the hydroxyl groups with an O···O distance of 2.620 Å. The weakly coordinated ethyl acetate molecules help fill the solvated channel space. The porphyrins interact through peripheral hydroxyl groups via strong directional hydrogen bonding and are arranged in an offset fashion with an interporphyrin vertical separation of 6.91 Å. The average hydrogen-bonding distance for O···O (HO···HO) is 2.75

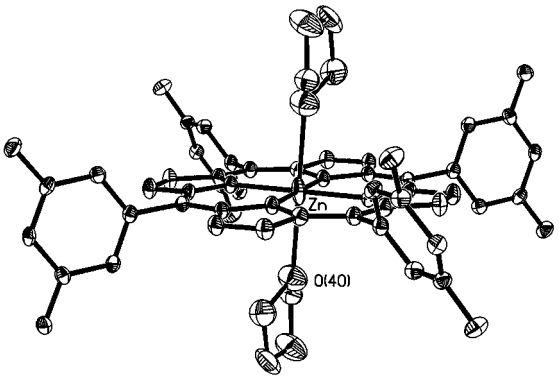

Figure 12. ORTEP diagram of the metalloporphyrin unit in the crystal structure of Zn[T(3′,5′-DHP)P](THF)$_2$·2THF·3CH_2Cl_2.

Å. Each layer is separated by a center-to-center distance of 11.00 Å. No hydrogen bonding was observed between the layers.

As seen with H_2T(2′,6′-DHP)P·4EtOAc, there exists an unusual interaction between the hydrogen-bonded porphyrin layers in Zn[T(2′,6′-DHP)P](EtOAc)$_2$·2EtOAc. *meso*-aryl rings of the adjacent layers are at a mismatched orientation with one aryl C−H pointing into the middle of another aryl ring on a porphyrin in the adjacent layer (Figure 11). The short distance of 2.71 Å from the aryl C−H to the adjacent porphyrin aryl-carbon indicates there is some C−H···π interactions between the layers.[12]

Zn[T(3′,5′-DHP)P](THF)$_2$·2THF·3CH_2Cl_2. Crystals were not forthcoming from Zn[T(3′,5′-DHP)P] in ethyl acetate, but

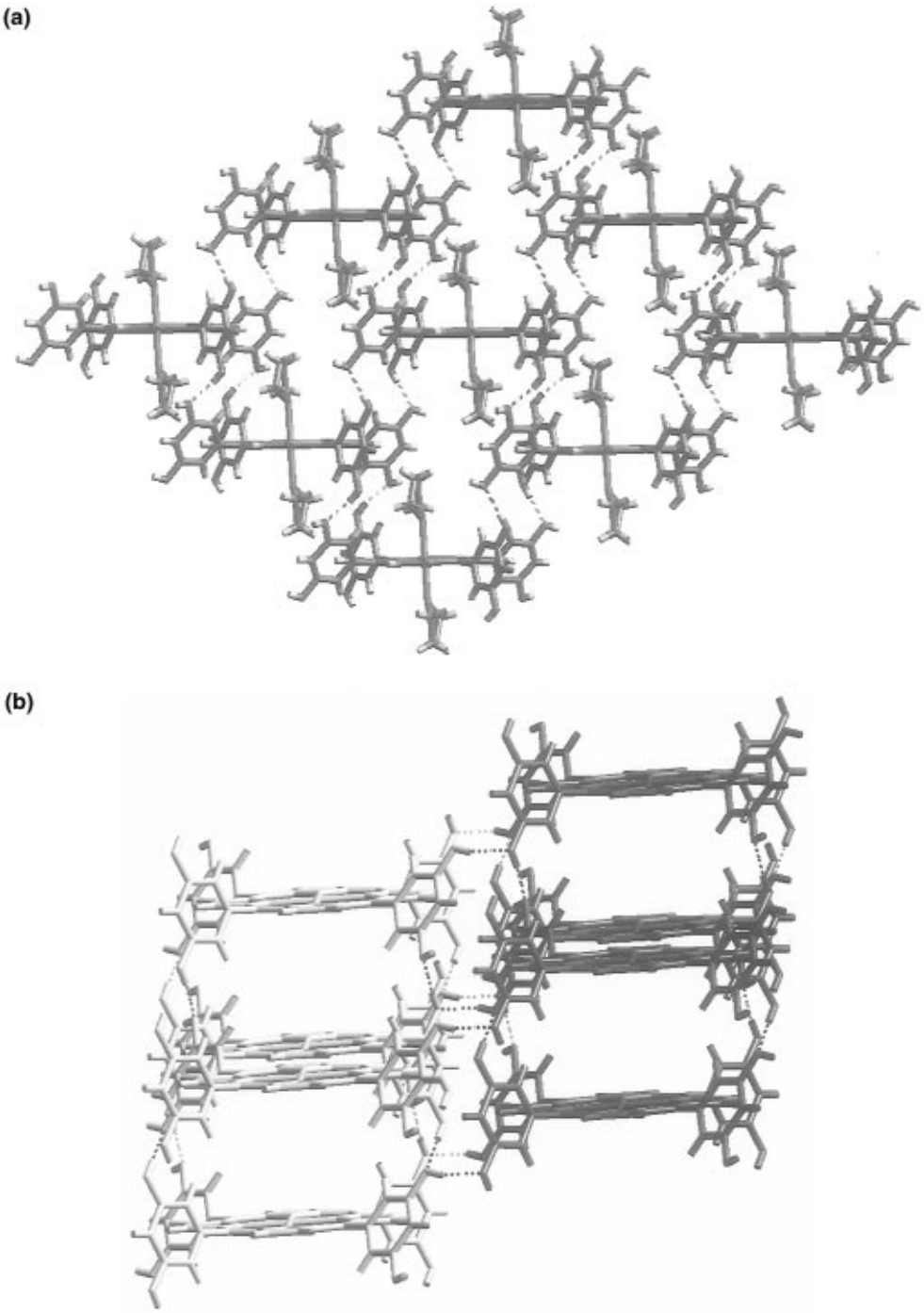

Figure 13. (a) Two-dimensional layer from the crystal structure of Zn[T(3′,5′-DHP)P](THF)$_2$·2THF·3CH_2Cl_2. Noncoordinated solvates are not shown for clarity. (b) Molecular packing diagram of Zn[T(3′,5′-DHP)P](THF)$_2$·2THF·3CH_2Cl_2 showing interconnected layers. Porphyrins in dark and light shades indicate two different layers. Hydrogen-bonding interactions are shown with dotted lines. Noncoordinated solvates are not shown for clarity.

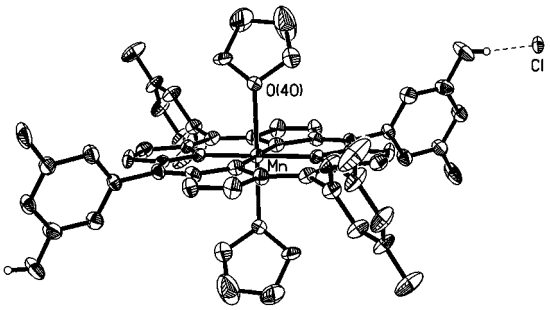

Figure 14. ORTEP diagram of the metalloporphyrin unit in the crystal structure of Mn[T(3′,5′-DHP)P](THF)$_2$·Cl·2THF·5$C_6H_5CH_3$.

were formed upon crystallization from THF. The porphyrin ring is planar with a six-coordinate geometry at the Zn(II) center. Two oxygen atoms of axial THF molecules are bonded to Zn-(II) center with a Zn−O distance of 2.44(2) Å (Figure 12). The average Zn−N distance in the equatorial plane is 2.045(3) Å.

A dramatic change in the crystal packing of H_2T(3′,5′-DHP)P arises with the inclusion of Zn(II) ion. The unit cell of Zn-[T(3′,5′-DHP)P](THF)$_2$·2THF·3CH_2Cl_2 has one porphyrin and *seven* solvate molecules (including the ligated THF). A molecular packing diagram showing a two-dimensional layered structure is shown in Figure 13a. Each porphyrin has four nearest hydrogen-bonded porphyrin neighbors. The interplanar separation between the hydrogen-bonded neighbors in a given layer is 6.81 Å. Within each layer the overlapping porphyrins are separated by 13.32 Å. The porphyrins are arranged in a slipped-stack orientation within the layer to maximize hydrogen-bonding interactions, with a mean O···O separation of 2.72 Å.

The two noncoordinated THF molecules are hydrogen bonded to the porphyrin OH groups. The (O···O) separation is 2.62 Å within the layers and 2.71 Å between the layers. Two layers are interconnected to give a three-dimensional structure, as shown in Figure 13b. The planes of the phenyl rings are offset between the adjacent layer, separated by a distance of 5.0 Å, and show negligible $\pi-\pi$ interaction. The nearest neighbor in the adjacent layer is offset by a vertical distance of 4.98 Å from the porphyrin plane. In this complex, the adjacent layers are held together by means of hydrogen-bonding interactions, while

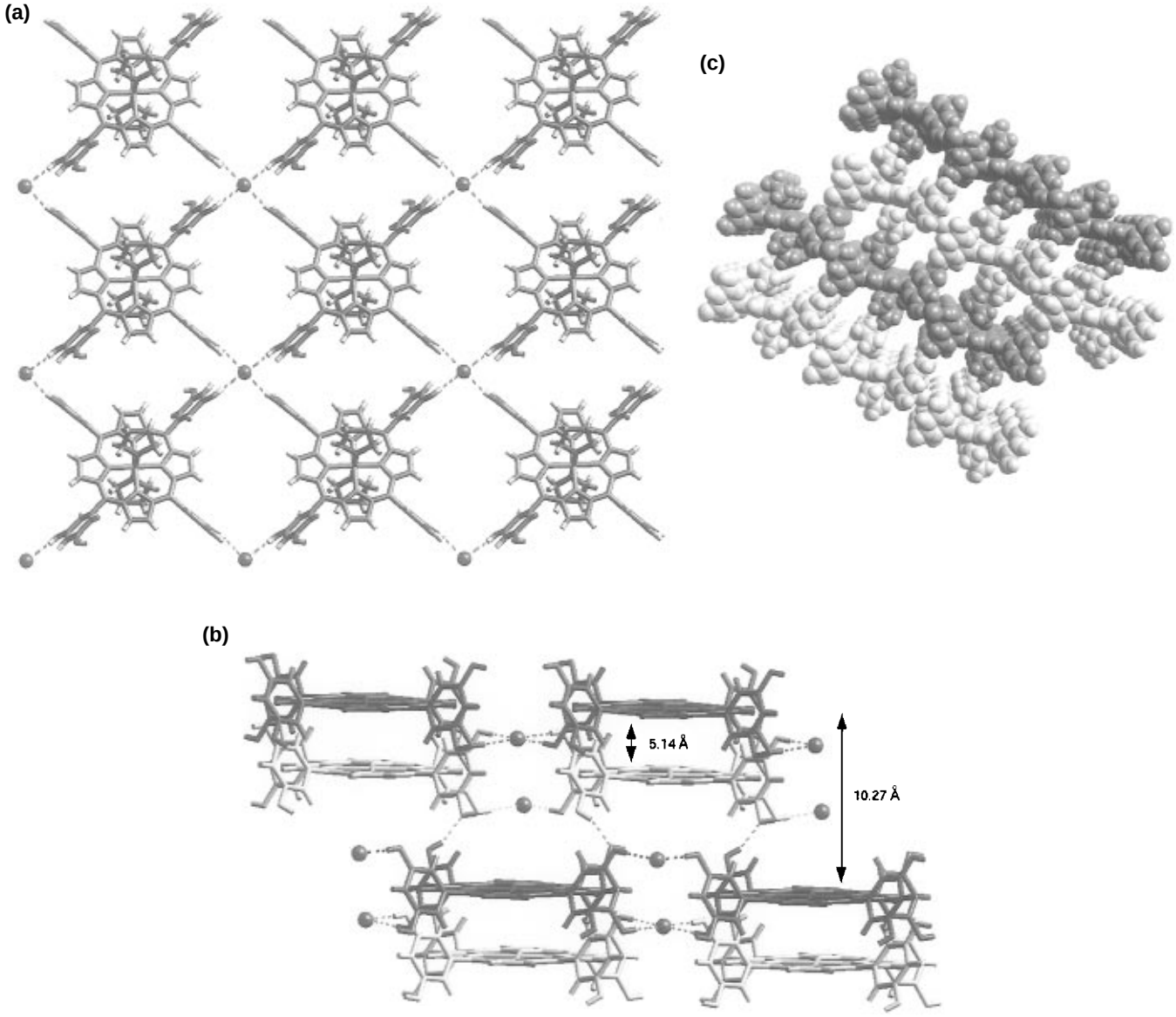

Figure 15. Molecular packing diagrams of Mn[T(3′,5′-DHP)P](THF)$_2$·Cl·2THF·5$C_6H_5CH_3$. The porphyrins in light and dark shades indicate farther away and front, respectively. (a) Two-dimensional sheets of porphyrins (001 plane) linked by unusual square-planar Cl^- anions hydrogen bonding to four metalloporphyrins. Spheres indicate bridging chloride ions. Solvate molecules and coordinated THF ligands are not shown for clarity. (b) A perpendicular view of the (100) plane showing interporphyrin hydrogen-bonding interactions. Spheres indicate bridging chloride ions. Solvate molecules and coordinated THF ligands are not shown for clarity. (c) Space-filled diagram showing channels of 4.6 Å × 3.4 Å (0.7 of their VDW atomic radii), viewed along the 100 plane (i.e., down the *b* axis). Noncoordinated solvates are not shown for clarity.

Table 1. Calculation of Channel Volumes for Various Porphyrin Complexes

porphyrin complex	*Z*	unit cell vol. (Å^3)	porphyrin vol./ unit cell[a] (Å^3)	solvate vol./ unit cell[a] (Å^3)	void vol./ unit cell[a] (Å^3)	total channel vol./ unit cell[b] (Å^3)
H_2TPP[c]	1	801.9	590.8	0	211	211 [26.3%]
H_2T(3′,5′-DHP)P·5EtOAc	1	1581	620.8	412.5	547.7	960.2 [60.7%]
H_2T(2′,6′-DHP)P·4EtOAc	2	2770.9	1233.0	660	877.9	1537.9 [55.5%]
H_2T(3′,5′-DHP)P·7C_6H_5CN	2	3811	1241.6	1547	1022	2569.4 [67.4%]
Zn[T(2′,6′-DHP)P](EtOAc)$_2$·2EtOAc	1	1387.2	804.1	168	415.2	583.2 [42.0%]
Zn[T(3′,5′-DHP)P](THF)$_2$·3CH_2Cl_2·2THF	1	1597.6	755.8	326.9	514.8	841.7 [52.7%]
Mn[T(3′,5′-DHP)P](THF)$_2$·Cl·2THF·5$C_6H_5CH_3$	2	4289	1612.2	1355	1321.8	2676.7 [62.4%]

[a] Porphyrin and solvate van der Waals volumes were calculated using Quanta for each unit cell. Void volume is defined as the unit cell volume minus the sum of the porphyrin volume and the solvate volume. For the metalloporphyrins, the volumes of the coordinated ligands were counted as part of the porphyrin volume. [b] Total channel volume is defined as the sum of void and solvate volume, in Å^3. Values in brackets refer to the percentage of total channel volume in the unit cell. [c] Crystallographic data is taken from ref 20.

the porphyrin layers in the H_2T(2′,6′-DHP)P·4EtOAc crystal lattice interact only with weaker van der Waals and C−H···π interactions.

Mn[T(3′,5′-DHP)P](THF)$_2$·Cl·2THF·5$C_6H_5CH_3$. Generally, Mn(III) porphyrin chloride derivatives retain Cl^- as the axial ligand, regardless of the solvent employed. They tend to show both five- and six-coordination geometry in the solid state depending on the crystallization solvent.[4,15−19] For example, even crystallization of MnTPP(Cl) from 1:1 benzene/pyridine solution does not displace the coordinated Cl^-, instead producing a six-coordinate complex with pyridine occupying the sixth coordination site.[16]

Surprisingly, for Mn[T(3′,5′-DHP)P]Cl, the Mn(III) porphyrin is six-coordinate with *two* axially ligated THF molecules (Figure 14). The average equatorial Mn−N distance is 2.004(2) Å, and the average axial Mn−O distance is 2.320(2) Å. A few six-coordinate complexes derived from MnTPP(ClO_4) have been reported in the literature, including [MnTPP(CH_3OH)$_2$](ClO_4),[17] [MnTPP(DMF)$_2$](ClO_4),[18] and [MnTPP(2,6-lutidine *N*-oxide)$_2$](ClO_4).[19]

A chloride ion bridges four hydroxyl groups from four different porphyrins in a square planar arrangement with an average Cl···O distance of 3.01 Å, as shown in Figure 15a,b. This unusual mode of anion coordination in Mn[T(3′,5′-DHP)P](THF)$_2$·Cl·2THF·5$C_6H_5CH_3$ is probably due to lattice stabilization by the hydrogen bonding between the Cl^- and HO groups.

Packing diagrams of Mn[T(3′,5′-DHP)P](THF)$_2$·Cl·2THF·5$C_6H_5CH_3$ are shown in Figure 15. In Figure 15a, one can see the two-dimensional porphyrin layers held together by the unusual square-planar Cl^- anions, each hydrogen bonding to four metalloporphyrin molecules. Figure 15b show that these layers are themselves interconnected through hydrogen bonding between metalloporphyrins of different layers, resulting in the three-dimensional network structure. The largest distance between the adjacent porphyrins within a layer is 10.27 Å, while a shortest distance between the offset porphyrins is 5.14 Å. The molecules are arranged alternatively in an offset fashion to give interconnected layers. The distance between the aryl rings of the adjacent porphyrins is greater than 4.69 Å, showing no $\pi-\pi$ interaction between the porphyrins. Within a given layer, the distance between Mn(III) centers is 16.44 Å, while a 13.13 Å separation is observed between two adjacent Mn(III) centers in different planes.

A space-filled molecular packing diagram shown in Figure 15c reveals 4.6 Å × 3.4 Å channels. There is a very large amount of solvate in the lattice. The five toluene molecules show some disorder, whereas the two unligated THF solvates are well ordered. The axially coordinated THF ligands partially fill the remaining void volume.

Molecular Modeling. To rationalize the crystal packing and the void space in these lattices, molecular modeling studies were performed on these structures. Molecular van der Waals radii of the solvate and the porphyrin or metalloporphyrin complex were calculated from energy-minimized structures. The total void volume of the unit cell was calculated by subtracting total solvate and porphyrin volumes from crystallographic unit cell volume and are summarized in Table 1. The porosity of these structures is striking. Even though porphyrin structures have been noted for high porosity, very few free base porphyrin structures show more than three solvates per porphyrin:[2,5] triclinic H_2TPP, for example, has *no* solvate.[20] As noted in Table 1, for these hydrogen-bonding porphyrins, the total channel volume is typically one-half to two-thirds of the total unit cell.

There is no systematic difference in void space for H_2T(2′,6′-DHP)P versus H_2T(3′,5′-DHP)P or their derivatives. Metal ions do not appear to influence void volume significantly, and the total channel volumes are comparable to the free base structures, if one counts the coordinated solvate ligands.

Conclusions

A series of two tetrakis(dihydroxyphenyl)porphyrins and their metal complexes have been explored as nanoporous supramolecular hydrogen-bonded network solids. The crystal structures for six such compounds have been determined. The self-assembly of these porphyrin networks is dominated by directional hydrogen bonding and is largely independent of $\pi-\pi$ interactions. Profound structural differences arise by simple permutation of phenyl substitution, solvate, and metal ion. Examples of one-dimensional columnar, two-dimensional layered, and three-dimensional network structures have all been found. In these structures, solvate-filled channels are observed with cross-sectional areas as large as 42 Å^2. The pore volumes

(15) (a) Cheng, H.; Scheidt, W. R. *Acta. Crystallogr.* **1996**, *C52*, 361. (b) Tulinsky, A.; Chen, B. M. L. *J. Am. Chem. Soc.* **1977**, *99*, 3647.
(16) Kirner, J. F.; Scheidt, W. R. *Inorg. Chem.* **1975**, *14*, 2081.
(17) Hatano, K.; Anzai, K.; Iitaka, Y. *Bull. Chem. Soc. Jpn.* **1983**, *56*, 422.
(18) Hill, C. L.; Williamson, M. M. *Inorg. Chem.* **1985**, *24*, 2836.
(19) Hill, C. L.; Williamson, M. M. *Inorg. Chem.* **1985**, *24*, 3024.
(20) Silvers, S. J.; Tulinsky, A. *J. Am. Chem. Soc.* **1967**, *89*, 3331.

of these channels are exceptionally large and can be as much as two-thirds of the total unit cell volume.

The present study demonstrates the effect of the directionality of the porphyrin substituents and size of the solvate on the supramolecular architectures of these molecules. We are currently exploring the possibility of using these supramolecular architectures in conjunction with the established reactivity of metalloporphyrins to create heterogeneous catalysts for shape selective oxidations.[21]

Acknowledgment. We thank Teresa Prussak for technical assistance in solving the crystal structures. This work was supported by the National Institute of Health (HL 5R01-25934) and in part by the DOE (DEFG0291ER45439).

Supporting Information Available: Tables of crystallographic data including atomic positional, thermal parameters, bond lengthes, and bond angles for all the six crystal structures (46 pages). See any current masthead page for ordering and Internet access instructions.

JA971093W

(21) (a) Suslick, K. S. In *Comprehensive Supramolecular Chemistry*; Bioinorganic Systems; Lehn, J. M., Ed.; Elsevier: London, 1996; Vol. 5, p 141. (b) Suslick, K. S.; Cook, B. R.; Fox, M. M. *J. Chem. Soc., Chem. Commun.* **1985**, 580. (c) Cook, B. R.; Reinert, T. J.; Suslick, K. S. *J. Am. Chem. Soc.* **1986**, *108*, 7281. (d) Suslick, K.; Cook, B. *J. Chem. Soc., Chem. Commun.* **1987**, 200. (e) Suslick, K. S.; Cook, B. R. Shape Selective Oxidation as a Mechanistic Probe. In *Inclusion Phenomena and Molecular Recognition*; Atwood, J. L., Ed.; Plenum Press: London, 1990; pp 209−215.